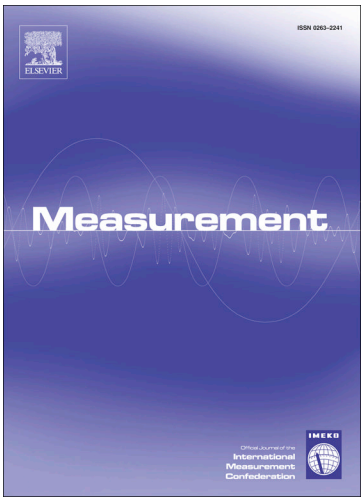


# Stochastic Digital DFT Processor and Its Application to Measurement of Reactive Power and Energy

Dragan Pejic, Dragana Naumovic-Vukovic, Bojan Vujicic, Aleksandar Radonjic, Platon Sovilj, Vladimir Vujicic

PII: S0263-2241(18)30279-3
DOI: https://doi.org/10.1016/j.measurement.2018.04.004
Reference: MEASUR 5405

To appear in: *Measurement*

Received Date: 22 June 2017
Revised Date: 27 March 2018
Accepted Date: 1 April 2018

Please cite this article as: D. Pejic, D. Naumovic-Vukovic, B. Vujicic, A. Radonjic, P. Sovilj, V. Vujicic, Stochastic Digital DFT Processor and Its Application to Measurement of Reactive Power and Energy, *Measurement* (2018), doi: https://doi.org/10.1016/j.measurement.2018.04.004

**the author's affiliations are as follows:**

**1. Dragan Pejic**
**Faculty of Technical Sciences, Department of Power, Electronic and Telecommunication Engineering**
**Trg Dositeja Obradovica 6**
**21000 Novi Sad**
**Serbia**

**2. Dragana Naumovic-Vukovic**
**Electrical Engineering Institute Nikola Tesla**
**Koste Glavinica 8a**
**11000 Beograd**
**Serbia**

**3. Bojan Vujicic**
**Faculty of Technical Sciences, Department of Power, Electronic and Telecommunication Engineering**
**Trg Dositeja Obradovica 6**
**21000 Novi Sad**
**Serbia**

**4. Aleksandar Radonjic**
**Institute of Technical Sciences of the Serbian Academy of Sciences and Arts**
**Knez Mihailova 35/IV**
**11000 Belgrade**
**Serbia**

**5. Platon Sovilj**

**Faculty of Technical Sciences, Department of Power, Electronic and Telecommunication Engineering**
**Trg Dositeja Obradovica 6**
**21000 Novi Sad**
**Serbia**

**6. Vladimir Vujicic**
**Institute of Technical Sciences of the Serbian Academy of Sciences and Arts**
**Knez Mihailova 35/IV**
**11000 Belgrade**
**Serbia**

# Stochastic Digital DFT Processor and Its Application to Measurement of Reactive Power and Energy

Dragan Pejic, Dragana Naumovic-Vukovic, Bojan Vujicic, Aleksandar Radonjic, Platon Sovilj and Vladimir Vujicic

***Abstract*-In this paper we present the model of digital stochastic DFT processor. Compared to the classical DFT/FFT processors, the proposed model has two advantages: first, it is much simpler and cheaper to implement, and second, it allows us to compute individual DFT components either in isolation or in parallel. In order to prove the validity of our model, we have simulated the measurement of reactive power and energy. In addition, we have conducted several experiments under field and laboratory conditions. The obtained results have shown that reactive power and energy can be measured with an accuracy of several ppm.**

***Keywords*: Stochastic measurements, DFT processor, reactive power, reactive energy.**

## 1. Introduction

The Discrete Fourier Transform (DFT) [1] is one of the most important procedures in the field of digital signal processing. It allows us to analyze and manipulate signals in ways not possible with analog signal processing. In practice, the DFT is usually computed using one of the Fast Fourier Transform algorithms (FFTAs). The most popular is probably the Cooley-

Tukey (CT) algorithm [2] or some of its derivatives [3], [4], [5]. This class of algorithms reduces the complexity of the DFT from $O(n^2)$ to $O(n \cdot \log n)$, which is a significant saving even when $n$ is relatively small. On the other hand, the computational simplicity of the CT-FFTA does not mean that it is easy to implement. Moreover, numerous studies (see [6], [7] and references herein) have shown that CT-FFT processors are very complex. The reason for this is that they are designed to process high-resolution samples of the input signal. In many cases, the resolution of the A/D converter (ADC) is 10 bits or even higher [6], [7].

Bearing this in mind, in this paper we extend the ideas presented in [15], [21], and propose an alternative approach to compute the DFT. Compared to FFTAs, the proposed approach has

**Table 1.** Notations used in this paper.

| Symbol | Meaning |
|---|---|
| $\Psi_i$ | Result of A/D conversion in channel $i$ ($i$ = 1, 2) |
| $\Delta_i$ | Quantum of the uniform quantizer in channel $i$ ($i$ = 1, 2) |
| $t_2 - t_1$ | Measurement interval |
| $N$ | Number of samples within measurement interval |
| $a_j$ | Cosine component of the $j$-th harmonic |
| $b_j$ | Sine component of the $j$-th harmonic |
| $n$ | Additive noise (in channel 1) |
| $p(n)$ | Probability density function of additive noise |
| $D/A$ | Digital-to-analog converter |
| $RNG$ | Random number generator |
| $Q_{(-\pi/2)}$ | Reactive power according to the IEEE/IEC |
| $Q_{(B)}$ | Budeanu's reactive power |

two advantages: first, it is much simpler and cheaper to implement, and second, it allows us to compute individual DFT components either in isolation or in parallel. Thanks to this, the measurement of any electrical quantity can be greatly simplified. In order to illustrate this, in this paper, we have simulated the measurement of average reactive power/energy (RP/RE) at the fundamental frequency and under nonsinusoidal conditions. Among many definitions of RP [8], [9], [10], we have chosen that of Budeanu [11]. Unlike the definition given by the IEEE [10], this definition does not require the introduction of a phase shift of $\pi/2$ between the voltage and current signals (at each harmonic frequency). At the same time, it is equivalent to that given by the IEEE (Appendix A). In addition, in the special case (when the phase angle between the first harmonic of the voltage and current is positive) it is also equivalent to that of Fryze [11] (Appendix A). Thus, our choice had no influence on the validity of obtained results.

The organization of this paper is as follows: Section 2 deals with the theoretical background of the stochastic digital DFT (SDDFT) processor. Experimental results and their discussion are

given in Section 3, while Section 4 presents one practical application of the proposed processor. Finally, Section 5 concludes the paper. For ease of reading, a list of notations is given in Table 1.

## 2. Stochastic Digital DFT Processor

*A. Theoretical Background*

The proposed processor is based on stochastic digital measurement method (SDMM) [12], [13], [14], [15], [16], [17], [18], [19], [20], [21], [22]. The main idea of this method consists in adding a random uniform dither to the input signal before its digitalization. For instance, if we want to measure the mean value of a product of two analog signals $f_1(t)$ and $f_2(t)$ (e.g. voltage and current [13]) it is necessary to add two uncorrelated dithers $h_1$ and $h_2$ (Fig. 1).

In that case, the output value $\overline{\Psi}$ will be equal to [14]

$$\overline{\Psi} = \frac{1}{N} \cdot \sum_{i=1}^{N} \Psi_1(i) \cdot \Psi_2(i) = \frac{1}{t_2 - t_1} \cdot \int_{t_1}^{t_2} f_1(t) \cdot f_2(t)\, dt \tag{1}$$

Accordingly, the variance of the average error $e$ will not be greater than [14]

$$\sigma_e^2 \le \frac{1}{N} \cdot \left[ \frac{\Delta_1^2}{4 \cdot (t_2 - t_1)} \cdot \int_{t_1}^{t_2} f_2^2(t)\, dt + \frac{{\Delta_2}^2}{4 \cdot (t_2 - t_1)} \cdot \int_{t_1}^{t_2} f_1^2(t)\, dt + \frac{\Delta_1^2 \cdot \Delta_2^2}{16} \right] \tag{2}$$

Using these results, the authors of [15] have shown that a two-channel instrument can be used to measure the harmonic component in the DFT. For that purpose it is necessary to replace the analog sum of the signals $f_2(t)$ and $h_2$ by memorized $m$-bit samples of a dithered (co)sine wave (Fig. 2). For instance, if $f_2(t) = R_2 \cdot \cos(j\omega t)$, the output value $\overline{\Psi}$ will be equal to

$$\overline{\Psi} = \frac{1}{t_2 - t_1} \cdot \int_{t_1}^{t_2} f_1(t) \cdot R_2 \cdot \cos(j\omega t)\, dt = \frac{R_2}{2} \cdot a_j = \frac{a_j}{2} \tag{3}$$

where $R_2 = 1$ represents the basis function range, while $\omega$ denotes the fundamental frequency. Analogously, if $f_2(t) = R_2 \cdot \sin(j\omega t)$, the output value $\overline{\Psi}$ will be equal to

$$\overline{\Psi} = \frac{1}{t_2 - t_1} \cdot \int_{t_1}^{t_2} f_1(t) \cdot R_2 \cdot \sin(j\omega t)\, dt = \frac{R_2}{2} \cdot b_j = \frac{b_j}{2} \tag{4}$$

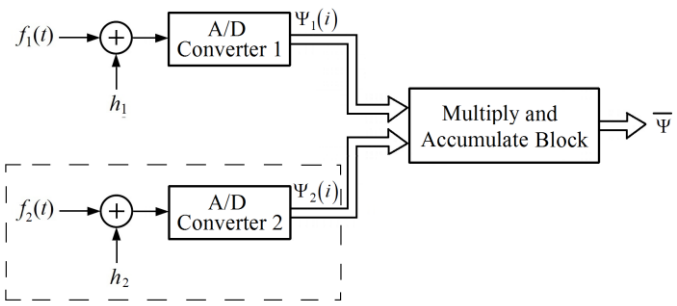


**Fig. 1**. The principal structure of a two-channel SDMM instrument.

The second important result from [15] concerns the variance of the average error *e*. Namely, since the signal $f_2(t)$ is a sine or cosine wave, it is clear that

$$\frac{1}{t_2 - t_1} \cdot \int_{t_1}^{t_2} f_2^2(t)\, dt = \frac{R_2^2}{2} = \frac{1}{2}. \tag{5}$$

As a result, the expression (2) reduces to

$$\sigma_{\bar{e}}^2 \le \frac{1}{N} \cdot \left[ \frac{\Delta_1^2}{8} + \frac{\Delta_2^2}{4 \cdot (t_2 - t_1)} \cdot \int_{t_1}^{t_2} f_1^2(t)\, dt + \frac{\Delta_1^2 \cdot \Delta_2^2}{16} \right] \tag{6}$$

where $\Delta_2 = R_2/(2^{m-1} - 1) = 1/(2^{m-1} - 1)$. To our best knowledge, the case when the instrument uses a two-bit stochastic flash A/D converter (SFADC) is not considered in the literature. This case, however, has a special significance for two reasons: first, a two-bit SFADC has the simplest hardware, and second, its output, $\Psi_1(i)$, has only three values: "- 1", "0" and "+ 1" (for more details see [12]). Thanks to this, the multiplication of samples $\Psi_1(i)$ and $\Psi_2(i)$ reduces to conditional sign change of $\Psi_2(i)$ or its annulment. In other words, there is no multiplication.

*B. Majorant Analysis*

In [15] it was suggested that the resolution of dithered base functions (DBFs) should be more than two bits greater than that of the applied ADC. In our case this means that the

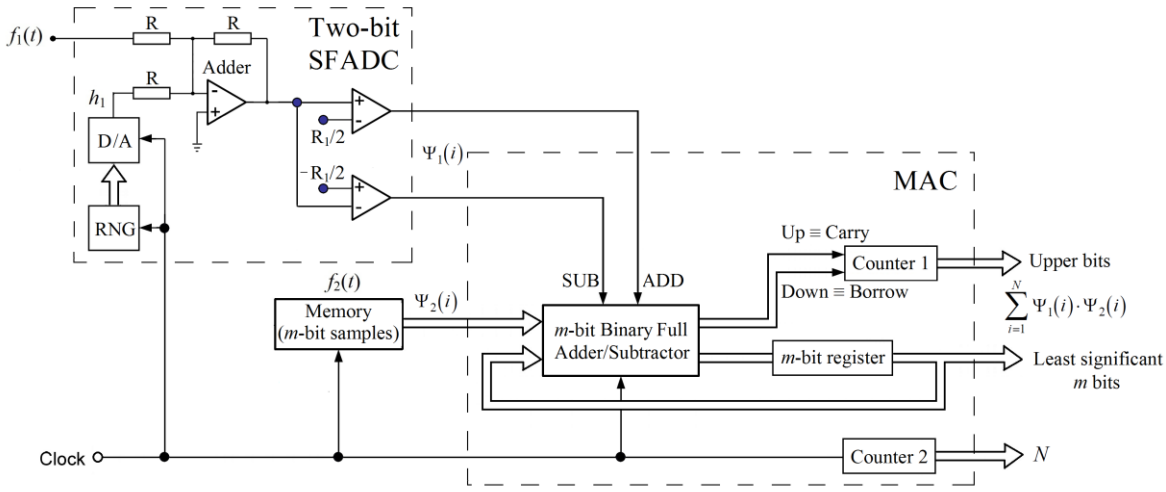


**Fig. 2**. General scheme for measurement one Fourier coefficient with a two-bit stochastic flash A/D converter (SFADC).

resolution of DBFs should be at least five bits. From the practical point of view, however, it is interesting to analyze the cases when the resolution of DBFs is *m* = 2, 3 and 4 bits. Such a scheme would be easy to implement, since almost all processing is performed by an *m*-bit binary

full adder/subtractor (Fig. 2). Given this, let us consider the scenario when the input signal is affected by additive noise. In that case, the expressions (1) and (6) will be transformed into

$$\bar{\Psi} = \frac{1}{N} \cdot \sum_{i=1}^{N} \Psi_1(i) \cdot \Psi_2(i) = \frac{1}{t_2 - t_1} \cdot \int_{t_1}^{t_2} dt \int_{-R_1}^{R_1} \left[ f_1(t) + n \right] \cdot f_2(t) \cdot p(n)\, dn \tag{7}$$

$$\sigma_{\bar{e}}^2 \le \frac{1}{N} \cdot \left[ \frac{\Delta_1^2}{8} + \frac{\Delta_2^2}{4 \cdot (t_2 - t_1)} \cdot \int_{t_1}^{t_2} dt \int_{-R_1}^{R_1} \left[ f_1(t) + n \right]^2 \cdot p(n)\, dn + \frac{\Delta_1^2 \cdot \Delta_2^2}{16} \right] \tag{8}$$

In addition, if one uses a two-bit SFADC, the expression (7) reduces to

$$\frac{1}{t_2 - t_1} \cdot \int_{t_1}^{t_2} dt \int_{-R_1}^{R_1} \left[ f_1(t) + n \right]^2 \cdot p(n)\, dn \le \frac{1}{t_2 - t_1} \cdot \int_{t_1}^{t_2} dt \int_{-R_1}^{R_1} R_1^2 \cdot p(n)\, dn \le \Delta_1^2 \tag{9}$$

while the absolute measurement uncertainty has the following limits:

1) $m = 2$ ($\Delta_2 = 1$)

$$\sigma_{\bar{e}} \le \sqrt{\frac{1}{N} \cdot \left[ \frac{\Delta_1^2}{8} + \frac{\Delta_1^2 \cdot \Delta_2^2}{4} + \frac{\Delta_1^2 \cdot \Delta_2^2}{16} \right]} = \frac{\Delta_1}{\sqrt{8N}} \cdot (1.87) \tag{10}$$

2) $m = 3$ ($\Delta_2 = 1/3$)

$$\sigma_{\bar{e}} \le \sqrt{\frac{1}{N} \cdot \left[ \frac{\Delta_1^4}{8} + \frac{\Delta_1^2 \cdot \Delta_2^2}{4} + \frac{\Delta_1^2 \cdot \Delta_2^2}{16} \right]} = \frac{\Delta_1}{\sqrt{8N}} \cdot (1.13) \tag{11}$$

3) $m = 4$ ($\Delta_2 = 1/7$)

$$\sigma_{\bar{e}}^2 \le \sqrt{\frac{1}{N} \cdot \left[ \frac{\Delta_1^4}{8} + \frac{\Delta_1^2 \cdot \Delta_2^2}{4} + \frac{\Delta_1^2 \cdot \Delta_2^2}{16} \right]} = \frac{\Delta_1}{\sqrt{8N}} \cdot (1.025) \tag{12}$$

If we take a look at the three analyzed majorant cases, we can see that the measurement uncertainty slightly depends on *m*, the resolution of memorized DBFs. On the other hand, from Fig. 2 it is clear that the value of the parameter *m* has a significant impact on the hardware complexity of the proposed processor. For instance, if DBF samples are stored in two-bit resolution, the multiply and accumulate (MAC) block will become very simple. More precisely, it will consist only of two counters and few logic gates (Fig. 3).

As illustrated on Fig. 2, the content of Counter 1 represents the sum of the product of two-bit samples, while the content of Counter 2 shows the number of measurement cycles in the interval $t_2 - t_1$. Of course, if we want to simultaneously measure $M$ Fourier coefficients, it is

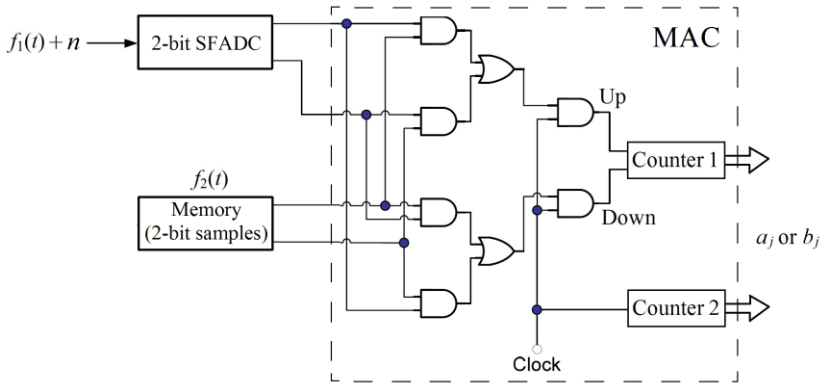


**Fig. 3**. Optimal scheme for measurement one Fourier coefficient with a two-bit SFADC.

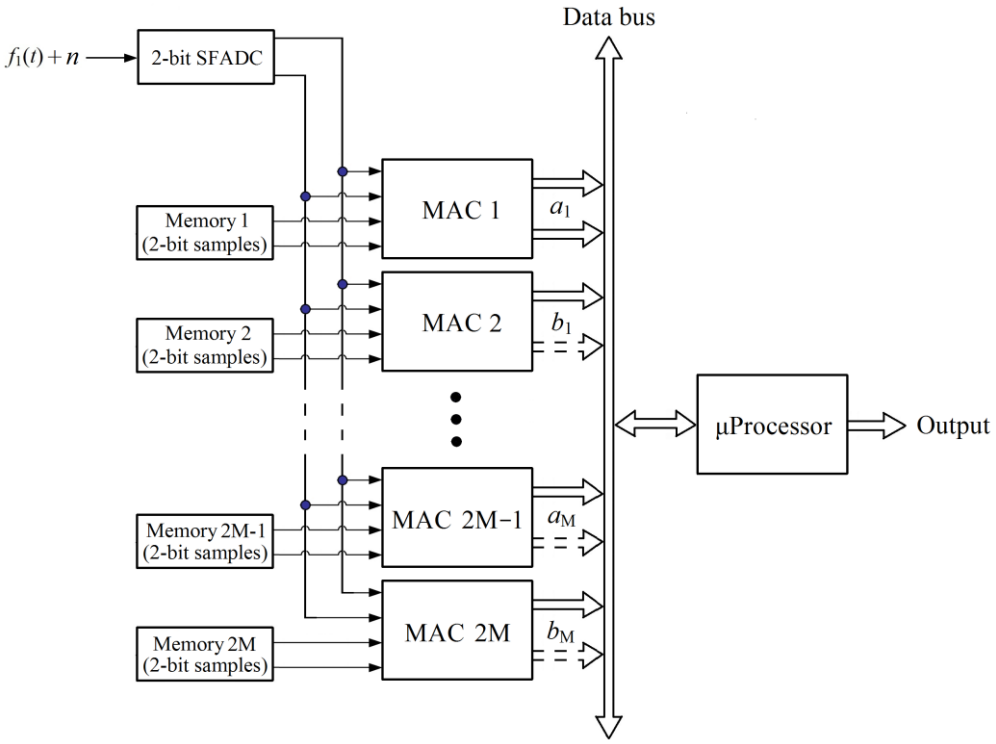


**Fig. 4.** Optimal SDDFT procesor for measurement 2*M* Fourier coefficients.

necessary to use 2*M* memory blocks, 2*M* Counters 1 and usually one Counter 2 (Fig. 4). The microprocessor is in charge of dividing the content of Counter 1 with the content of Counter 2. In this way one obtains Fourier coefficients, i.e.

$$a_j = \frac{2 \cdot <\text{Counter}1_{2j-1}>}{<\text{Counter}2_{2j-1}>} \tag{13}$$

$$b_j = \frac{2 \cdot <\text{Counter}1_{2j}>}{<\text{Counter}2_{2j}>} \tag{14}$$

## 3. Measurement of Reactive Power and Energy Using SDDFT Processor

The proposed processor can be used for various kinds of measurements. One of the most challenging applications is the measurement of RE. By knowing this quantity the utility companies can take the proper steps to reduce revenue losses and increase the power generation capacity.

*A. Reactive Power and Fourier Coefficients*

Suppose that the voltage and current signals, $u(t)$ and $i(t)$, are accurately approximated with *M*-order trigonometric polynomials

$$u(t) = \sum_{j=1}^{M} \left[ a_j \cdot cos(j\omega t) + b_j \cdot sin(j\omega t) \right] \tag{15}$$

$$i(t) = \sum_{j=1}^{M} \left[ c_j \cdot cos(j\omega t) + d_j \cdot sin(j\omega t) \right] \tag{16}$$

In that case, the RP can be calculated using the expression (Appendix A):

$$Q_{(-\pi/2)} = \sum_{j=1}^{M} Q_{j\,(-\pi/2)} = \sum_{j=1}^{M} \frac{a_j d_j - b_j c_j}{2} = \sum_{j=1}^{M} Q_{j\,(B)} = Q_{(B)} \tag{17}$$

From (17) we see that the RP can be expressed as a function of Fourier coefficients. In essence, this means that each harmonic RP component can be calculated by measuring only four Fourier coefficients. For instance, for $j$ = 1, the RP at the fundamental frequency (50/60Hz) can be calculated using the equality

$$Q_1 = \frac{a_1 \cdot d_1 - b_1 \cdot c_1}{2}. \tag{18}$$

Analogously we can compute the RP at double fundamental frequency, triple fundamental frequency and so on. In addition, we note that the expression (18) is valid for both Budeanu's and IEEE's definition of RP at the fundamental frequency (Appendix A).

*B. Simulation Results*

In [16] it was shown that the frequency distribution in European Interconnection is of Gaussian type with the mean of 49,9941 Hz and the standard deviation of 0,0204 Hz. However, as modern digital phase-locked loops have negligible settling time (few tens of $\mu$s [24]), and can provide the same number of samples per period of the measured signal, it is sufficient to simulate the measurement of average RP at 50 Hz (from the perspective of the SDDFT processor, the constant number of samples per period is equivalent to the situation when the frequency is constant). For that purpose, we have used the method described in [23]. In the first step, we have modeled the SDDFT processor that measures four Fourier coefficients: $a_1$, $b_1$, $c_1$ and $d_1$ (its parameters are set according to Table 2). In addition, the sources of systematic errors were simulated (it was set that both the analog adder and the comparators within the voltage/current ADC had 5 mV offset) as well as the method for their partial reduction [22] (the method proposed in [22] eliminates the comparators' offset).

In the second step, we have performed a series of simulations for the four following scenarios:

1) the voltage signal $u(t)$ is noisy, non-stationary and dithered ($f_s$ = 1 MHz, $N_s$ = 120),

2) the voltage signal $u(t)$ is noisy, non-stationary and non-dithered ($f_s$ = 1 MHz, $N_s$ = 120),

**Table 2.** Simulation parameters.

| | |
|---|---|
| *Number of simulations* | $N_S$ = 40 or 120 |
| *Signal-to-noise ratio* | SNR = 58 dB |
| *Input range of a two-bit voltage A/D converter* | $R_u$ = ± 2 V |
| *Input range of memorized m-bit (m = 2, 3, 4) voltage DBFs* | $R_u$ = ± 1 V |
| *Input range of a two-bit current A/D converter* | $R_i$ = ± 2 A |
| *Input range of memorized m-bit (m = 2, 3, 4) current DBFs* | $R_i$ = ± 1 A |
| *Input range of a 16-bit voltage D/A converter* | $R_{(u)}$ = ± 1 V |
| *Input range of a 16-bit current D/A converter* | $R_{(i)}$ = ± 1 A |
| *Sampling frequency* | $f_s$ = 1 MHz or 10 MHz |
| *Measurement interval* | $T$ = (300 x 20) ms |

3) the voltage signal $u(t)$ is noisy, stationary and dithered ($f_s$ = 1 MHz, $N_s$ = 120),

4) the voltage signal $u(t)$ is noisy, non-stationary and dithered ($f_s$ = 10 MHz, $N_s$ = 40).

In the first, second and fourth scenario, the voltage signal had the form

$$u(t)=(U_m/2)\cdot[1-(1000\pi t)/(6\cdot 142^2)]\cdot sin(2\pi\cdot 50\cdot t)+(U_m/2)\cdot[1-(1000\pi t)/(6\cdot 142^2)]\cdot sin(2\pi\cdot 150\cdot t) \quad (19)$$

i.e.,

$$u(t) = (U_m/2)\cdot(1 - 0.025967t)\cdot sin(2\pi\cdot 50\cdot t) + (U_m/2)\cdot(1 - 0.025967t)\cdot sin(2\pi\cdot 150\cdot t) \quad (20)$$

(the amplitudes of the voltage harmonics decrease linearly by 2.6 percent per second), while in the third scenario it had the form

$$u(t) = (U_m/2)\cdot[1-(1000\pi)/(2\cdot 142^2)]\cdot sin(2\pi\cdot 50\cdot t)+(U_m/2)\cdot[1-(1000\pi)/(2\cdot 142^2)]\cdot sin(2\pi\cdot 150\cdot t) \quad (21)$$

i.e.,

$$u(t) = (U_m/2)\cdot 0.92209897\cdot sin(2\pi\cdot 50\cdot t) + (U_m/2)\cdot 0.92209897\cdot sin(2\pi\cdot 150\cdot t) \quad (22)$$

where $U_m$ = 1.9 V. On the other hand, in all four scenarios, except the second one, the current signal was stationary and dithered (in the second scenario the current signal was stationary and non-dithered), and it had the form

$$i(t) = (I_m/2)\cdot sin(2\pi\cdot 50\cdot t + \pi/6) + (I_m/2)\cdot sin(2\pi\cdot 150\cdot t + \pi/9) \quad (23)$$

where $I_m$ = 1.9 A.

By analyzing the obtained results (Tables 3-6), we observe that in the second scenario the average measured value of $Q_1$ ($\overline{Q_{1m}}$) (Table 4) is quite different from both corresponding values of $\overline{Q_{1m}}$ in other scenarios (Tables 3, 5 and 6) and the average correct value of $Q_1$ ($\overline{Q_{1c}}$). The reason for this is the absence of dithered signals $h_1$ and $h_2$, which reduce the quantization errors. In addition, we also see that in the second scenario the standard deviation($\sigma_{\overline{Q_{1m}}}$) has the smallest

**Table 3.** Results of the first simulated scenario.

| $m$ | $\overline{Q_{1m}}$ [var] | $\overline{Q_{1c}}$ [var] | $\sigma_{\overline{Q_{1m}}}$ [var] | $\Gamma = \sigma_{\overline{Q_{1m}}} / \lvert\overline{Q_{1c}}\rvert$ |
|---|---|---|---|---|
| 4 | - 0.208015 | - 0.208049 | 0.000312 | 0.0015 |
| 3 | - 0.208085 | - 0.208049 | 0.000350 | 0.0017 |
| 2 | - 0.208053 | - 0.208049 | 0.000379 | 0.0017 |

**Table 4.** Results of the second simulated scenario.

| $m$ | $\overline{Q_{1m}}$ [var] | $\overline{Q_{1c}}$ [var] | $\sigma_{\overline{Q_{1m}}}$ [var] | $\Gamma = \sigma_{\overline{Q_{1m}}} / \lvert\overline{Q_{1c}}\rvert$ |
|---|---|---|---|---|
| 4 | - 0.277794 | - 0.208049 | 0.000036 | 0.000173 |
| 3 | - 0.277777 | - 0.208049 | 0.000080 | 0.000385 |
| 2 | - 0.277811 | - 0.208049 | 0.000283 | 0.001019 |

**Table 5.** Results of the third simulated scenario.

| $m$ | $\overline{Q_{1m}}$ [var] | $\overline{Q_{1c}}$ [var] | $\sigma_{\overline{Q_{1m}}}$ [var] | $\Gamma = \sigma_{\overline{Q_{1m}}} / \lvert\overline{Q_{1c}}\rvert$ |
|---|---|---|---|---|
| 4 | - 0.208059 | - 0.208049 | 0.000313 | 0.0015 |
| 3 | - 0.208054 | - 0.208049 | 0.000345 | 0.0017 |
| 2 | - 0.208102 | - 0.208049 | 0.000441 | 0.0021 |

**Table 6.** Results of the fourth simulated scenario.

| $m$ | $\overline{Q_{1m}}$ [var] | $\overline{Q_{1c}}$ [var] | $\sigma_{\overline{Q_{1m}}}$ [var] | $\Gamma = \sigma_{\overline{Q_{1m}}} / \lvert\overline{Q_{1c}}\rvert$ |
|---|---|---|---|---|
| 4 | - 0.208080 | - 0.208049 | 0.000112 | 0.00054 |
| 3 | - 0.208071 | - 0.208049 | 0.000109 | 0.00052 |
| 2 | - 0.208095 | - 0.208049 | 0.000096 | 0.00046 |

value. This result is also expected due to the absence of the dithered signal. On the other hand, we see that in all other scenarios the values of $\overline{Q_{1m}}$ are practically the same regardless whether the voltage signal is stationary or not (Tables 3, 5 and 6). The same applies for the values of $\sigma_{\overline{Q_{1m}}}$, except in the case of the fourth scenario (Table 6). In this scenario the value of $\sigma_{\overline{Q_{1m}}}$ is $\sqrt{10}$ times lower because of 10 times higher sampling frequency. Further, it is interesting to analyze the results in the case of the third scenario (when the sources of systematic errors are disabled) (Table 5). Namely, by comparing these results with those given in Tables 3 and 6, we see that the sources of systematic errors have no impact on the measurement precision and accuracy. In addition, we note that the third simulated scenario was characterized by the following standard deviations (within one signal period): $\sigma = 0{,}0056$ for $m$ = 4, $\sigma = 0{,}0058$ for $m$ = 3, and $\sigma = 0{,}0071$ for $m$ = 2. However, as the $Q_1$ was successively measured in 300 periods, the corresponding variance was equal to $\sigma_{\overline{Q_{1m}}} \approx \sigma / \sqrt{300}$ (Table 5).

Besides this, it is important to note that the above considerations apply to the measurement of RE due to two things: first, the RE is the accumulation of RP over time, and second, the uncertainty of the time measurement is extremely low (Appendix B). In practice, the RE is always measured in very long period of time. On the basis of data given in Tables 3, 5 and 6 it easy to conclude that, in a period of one day, the value of $\bar{Q}_1$ can be measured with the precision of 14 ppm ($0.17/\sqrt{86400/6}\% = 0.0014\,\%$). According to the central limit theorem, in a period of one month, the imprecision will decrease with $\sqrt{30}$, i.e. it will be 2.6 ppm. If contemporary ADC and D/A converters (DACs) [25], [26] were used, the sampling frequency could be increased to 2 GHz. As a result, in a measurement period of one month, the measurement precision would be $\sqrt{200}$ times lower, i.e. it would be equal to 0.18 ppm.

*C. Laboratory Experiments*

To validate simulation results, we have conducted several laboratory experiments. For that purpose, two instruments were used: the quadruple three-phase power analyzer called MM4 (Fig. 5a) and the phase angle standard (PAS) (Fig. 5b) [27].

The heart of the first instrument is a two-bit SDDFT processor. It was implemented in two FPGA chips and enables each MM4 to measure up to 70 quantities:

1) 3 voltage RMS (with the accuracy of 0.2 % of full scale) [12],

2) 16 current RMS (with the accuracy of 0.2 % of full scale) [12],

3) 12 active powers (with the accuracy of 0.5 % of full scale) [12],

4) 38 fundamental Fourier coefficients (with the accuracy of 0.2 % of full scale) [21],

5) power grid frequency (with the accuracy of 0.02 % of full scale) [20].

The instrument operates at a sampling frequency of 0.5 MHz and has a peak performance of 2.2 GFLOPS. In addition, it is connected to the PC via the USB cable. The reason for this is twofold: first, the PC provides an adequate visual representation of the measured data, and second, it is used to calculate both Fryze's RP in the $R_1$-phase and the fundamental of Budeanu's RP in the $R_1$-phase (based on the measured values of fundamental Fourier coefficients).

The second instrument has several functional blocks including two-channel digital function generator. In our experiments, this block was used as standard signal generator. Its main characteristics are as follows:

1) frequency range 10 Hz–10 kHz,

2) voltage range 0–120 V,

3) current range 0–6 A,

4) output power: voltage channel 25 W, current channel 100 W,

6) phase angle: 0º–360º,

7) phase angle resolution: equivalent to time delay of 5 ns in high-speed operation.

The experiments were started by generating the same signals as those in the first, third and fourth scenario (the experiment for the second scenario was not conducted due to impossibility


(a) (b)

**Fig. 5**. Photos of the instruments used in laboratory experiments:
(a) a two-bit quadruple three-phase power analyzer (MM4) and (b) the phase angle standard (PAS).

of switching-off dithered signals). Because of limited capacity of the PAS's EEPROM, all signals were generated on a period-by-period basis. Unlike simulation experiments, the sampling frequency was 0.5 MHz, which is the operating frequency of the MM4. After finishing all the experiments, the obtained results were firstly normalized (with respect to the dynamic ranges of both the MM4 and the PAS) and then averaged. As Table 7 shows, experimental results are still

within theoretical bounds. More precisely, in the first and third scenario the values of $\sigma_{\overline{Q_{1m}}}$ are about $\sqrt{150} \approx 12$ times lower than those obtained through simulations. The reason for this is twofold: first, the sampling frequency is 2 times lower than that used in the simulations (0.5 MHz versus 1 MHz), and second, an additional averaging the values of $Q_{1m}$ (across all 300 periods) was performed. The similar applies to results obtained in the fourth scenario: they were generated by averaging the results of 10 experiments. Finally, it could be noted that the difference between the values of $\overline{Q_{1m}}$ and $\overline{Q_{1c}}$ is far less than (conservatively) declared accuracy of the MM4 (which is 0.4 % of the full scale).

## 4. One Practical Application of the SDDFT Processor

**Table 7.** Results of the laboratory experiments.

| Scenario | $\overline{Q_{1m}}$ [var] | $\overline{Q_{1c}}$ [var] | $\sigma_{\overline{Q_{1m}}}$ [var] | $\Gamma = \sigma_{\overline{Q_{1m}}} / \lvert\overline{Q_{1c}}\rvert$ |
|---|---|---|---|---|
| 1 | - 0.2084 | - 0.20805 | 0.000032 | 0.00015 |
| 2 | Impossible to validate with MM4 | | | |
| 3 | - 0.2083 | - 0.20805 | 0.000038 | 0.00018 |
| 4 | - 0.2083 | - 0.20805 | 0.000011 | 0.00006 |

In this section, we illustrate a practical application of a two-bit SDDFT processor. As an integral part of the MM4, it was recently used to verify the performances of the conventional measurement equipment (of the 0.2 accuracy class) installed in a big chemical processing plant. The measurements were performed at 2 second intervals over a period of 500 minutes. The obtained results are shown on Figs. 6-13 and Table 8.

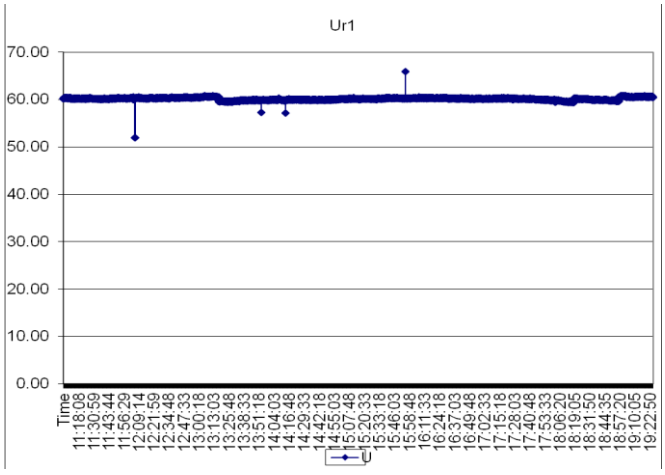


**Fig. 6**. The voltage in the $R_1$-phase ($U_{r1}$) as a function of time.

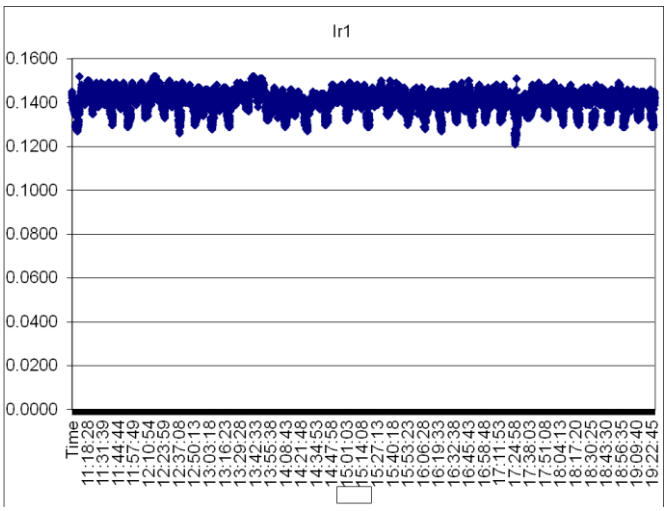


**Fig. 7**. The current in the $R_1$-phase ($I_{r1}$) as a function of time.

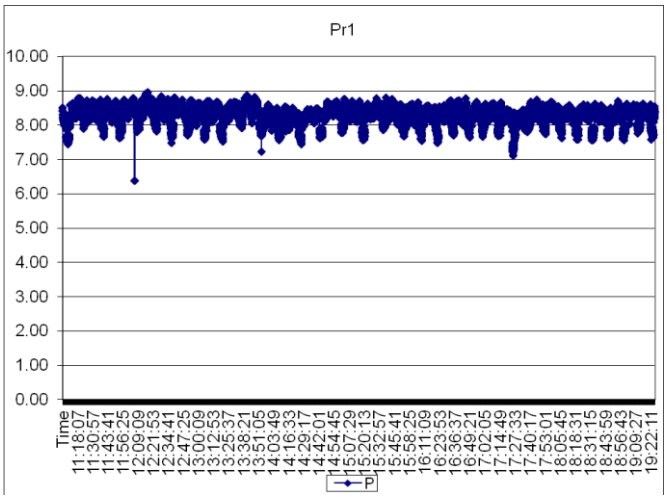


**Fig. 8**. The active power in the $R_1$-phase ($P_{r1}$) as a function of time.

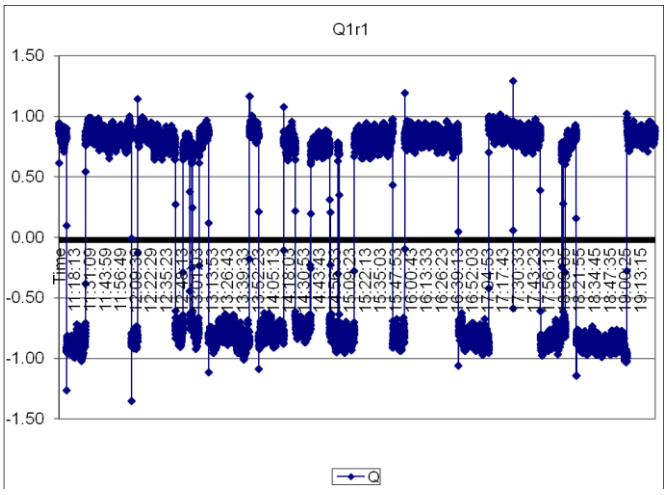


**Fig. 9**. The fundamental reactive (Budeanu's) power in the $R_1$-phase ($Q_{1r1}$) as a function of time.

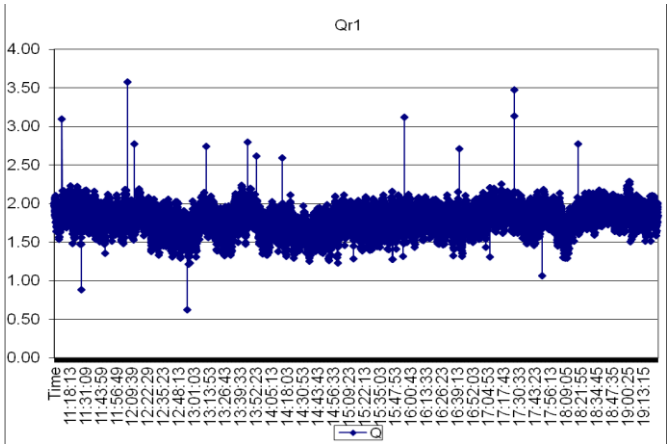


**Fig. 10**. Fryze's reactive power in the $R_1$-phase ($Q_{r1}$) as a function of time.

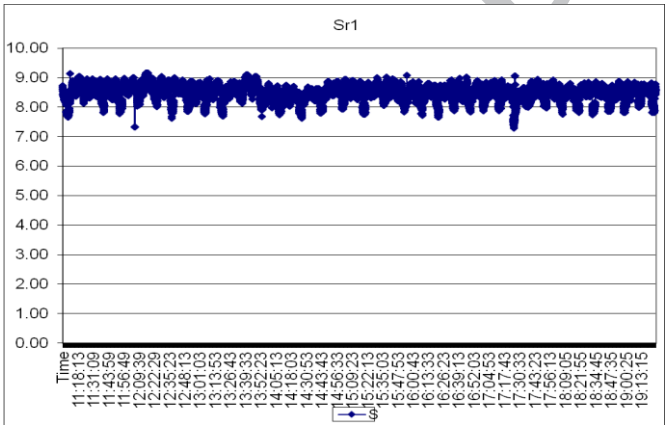


**Fig. 11**. The apparent power in the $R_1$-phase ($S_{r1}$) as a function of time.

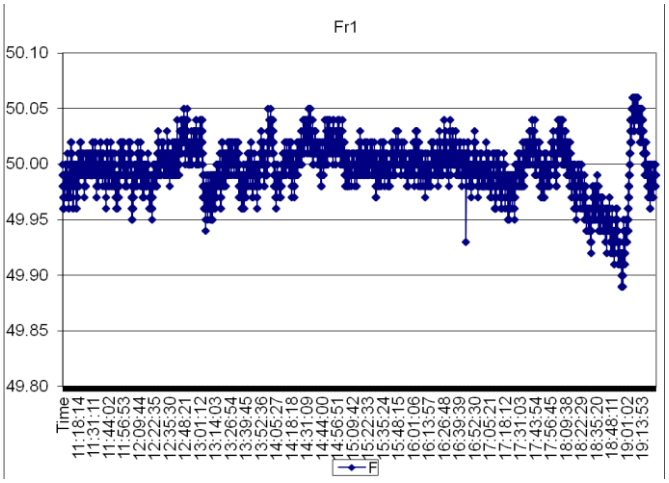


**Fig. 12**. The power grid frequency in the $R_1$-phase ($f_{r1}$) as a function of time.

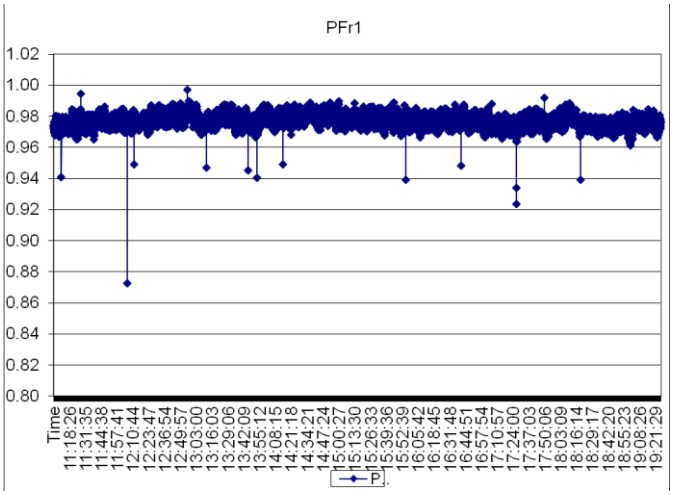


**Fig. 13**. The power factor in the $R_1$-phase ($PF_{r1}$) as a function of time.

**Table 8.** The minimum, average and maximum values of the measured quantities.

| | $U_{r1}$ [V] | $I_{r1}$ [A] | $P_{r1}$ [W] | $Q_{r1}$ [var] | $Q_{1r1}$ [var] | $S_{r1}$ [VA] | $f_{r1}$ [Hz] | $PF_{r1}$ |
|---|---|---|---|---|---|---|---|---|
| Minimum value | 51.93 | 0.121 | 6.39 | 0.62 | - 1.35 | 7.30 | 49.89 | 0.873 |
| Average value | 60.16 | 0.141 | 8.29 | 1.80 | 0.10 | 8.49 | 50.00 | 0.977 |
| Maximum value | 65.86 | 0.152 | 8.96 | 3.57 | 1.29 | 9.16 | 50.06 | 0.997 |
| Standard deviation | 0.27 | 0.04 | 0.25 | 0.16 | 0.82 | 0.25 | 0.02 | 0.004 |

Frize's RP has the highest value of all defined RPs. Today, mainly on Frize's definition, an orthogonal decomposition of apparent power (AP) is performed in several various ways [28], [29], [30], [31], [32]. Besides the active power P, in all orthogonal decompositions one of the orthogonal components of AP is Budeanu's RP (denoted in Appendix A as $Q_{(B)}$). In industrial applications the most important component of Budeanu's RP (that at the fundamental frequency) can easily be compensated using parallel capacitive compensators. This is confirmed in this practical case (Fig. 9 and Table 8) - the average value of Budeanu's RP at the fundamental frequency is 0.1 var, which is practically negligible.

Finally, in [33] it was shown that measurement of the rms of three (inter) phase voltages, the rms of three phase currents, the fundamental harmonics of three (inter) phase voltages and the fundamental harmonics of three phase currents is sufficient to measure power and energy according to the IEEE Std 1459-2010 [34]. All these quantities can be also measured with the MM4. An experimental illustration of this, however, is a topic beyond the scope of this paper.

## 5. Conclusion

In this paper, the model of digital stochastic DFT processor was presented. The presented model is theoretically analyzed and practically verified through simulations and experiments. The obtained results demonstrate that the optimal processor has a two-bit resolution as well as

that its precision increases with the square root of the number of digitized samples. Furthermore, it is shown that the proposed processor is well suited for parallel long-lasting measurements. For instance, by using contemporary ADCs and DACs, the electrical quantities, such as reactive power and energy, can be measured with an accuracy of several ppm. Thanks to this feature, the proposed stochastic digital DFT processor represents a solid basis for the design of high-precision power and energy measurement instruments as an alternative to those based on FFT or other spectral methods.

## References


[1] G. D'Antona and A. Ferrero, Digital Signal Processing for Measurement Systems: Theory & Applications, Springer Science Inc., 2006.

[2] J. Cooley and J. Tukey, "An Algorithm for the Machine Computation of the Complex Fourier Series," *Math. Computation*, vol. 19, no. 90, pp. 297-301, Apr. 1965.

[3] R. Mersereau and T. Speake, "A Unified Treatment of Cooley-Tukey Algorithms for the Evaluation of the Multidimensional DFT," *IEEE Trans. Acoust. Speech Signal Process.*, vol. 29, no. 5, pp. 2430-2438, Oct. 1981.

[4] R. Bernardini *et al.*, "A Sequential Multidimensional Cooley-Tukey Algorithm," *IEEE Trans. Signal Process.*, vol. 42, no. 9, pp. 205-222, Sep. 1994.

[5] Y. Voronenko and M. Puschel, "Algebraic Signal Processing Theory: Cooley-Tukey Type Algorithms for Real DFTs," *IEEE Trans. Signal Process.*, vol. 57, no. 1, pp. 205-222, Jan. 2009.

[6] T. Lenart and V. Öwall, "Architectures for Dynamic Data Scaling in 2/4/8K Pipeline FFT cores," *IEEE Trans. Very Large Scale Integr. (VLSI) Syst*., vol. 14, no. 11, pp. 1286-1290, Nov. 2006.

[7] H.-Y. Lee and I.-C. Park, "Balanced Binary-Tree Decomposition for Area-Efficient Pipelined FFT Processing," *IEEE Trans. Circuits Syst. I, Reg. Papers*, vol. 54, no. 4, pp. 889-900, Apr. 2007.

[8] M. E. Balci, M. H. Hocaoglu, "Comparison of Power Definitions for Reactive Power Compensation in Nonsinusoidal Conditions", *Proc. 11th Int. Conf. on Harmonics and Quality of Power*, pp. 519-524, Sept. 2004.

[9] I. Masoudipour, H. Samet, "Comparison of Various Reactive Power Definitions in Non-Sinusoidal Networks with the Practical Data of Electrical Arc Furnace", *Proc. 22th Int. Conf. on Electricity Distribution*, Paper no. 1256, June 2013.

[10] *IEEE Standard Dictionary of Electrical and Electronics Terms*, 4th ed. New York: IEEE, 1988. ANSI/IEEE Std. 100-1988.

[11] A. E. Emanuel, Power Definitions and the Physical Mechanism of Power Flow, John Wiley & Sons, Ltd., 2010.

[12] V. Vujicic *et al.*, "Low Frequency Stochastic True RMS Instrument," *IEEE Trans. Instrum. Meas.*, vol. 48, no. 2, pp. 467-470, Apr. 1999.

[13] D. Pejic and V.Vujicic, "Accuracy Limit of High-Precision Stochastic Watthour Meter," *IEEE Trans. Instrum. Meas.*, vol. 49, no. 3, pp. 617-620, Jun. 2000.

[14] V. Vujicic, "Generalized Low-Frequency Stochastic True RMS Instrument," *IEEE Trans. Instrum. Meas.*, vol. 50, no. 5, pp. 1089-1092, Oct. 2001.

[15] V. Pjevalica and V. Vujicic, "Further Generalization of Low-Frequency True-RMS Instrument," in *Proc. IMTC*, May 2005, pp. 1008–1011.

[16] Z. Beljic *et al.*, "Grid Fundamental Harmonic Measurement in Presence of Gaussian Frequency Deviation using 2-bit Flash A/D Converter", *Technical Gazette*, vol. 24, no. 2, pp. 481-488, Apr. 2017.

[17] B. Santrac *et al.*, "A Novel Method for Stochastic Measurement of Harmonics at Low Signal-to-Noise Ratio," *IEEE Trans. Instrum. Meas.*, vol. 58, no. 10, pp. 3434-3441, Oct. 2009.
[18] P. Sovilj, S. Milovancev, and V. Vujicic, "Digital Stochastic Measurement of a Nonstationary Signal with an Example of EEG Signal Measurement," *IEEE Trans. Instrum. Meas.*, vol. 60, no. 9, pp. 3230-3232, Sep. 2010.
[19] A. Radonjic, P. Sovilj and V. Vujicic, "Measurement Uncertanity Bounds of DSM Method", *Proc. IEEE Conf. on Precision Electromagnetic Measurements (CPEM) 2012*, pp. 572-573, July 2012.
[20] A. Radonjic, P. Sovilj and V. Vujicic, "Stochastic Measurement of Power Grid Frequency Using a Two-Bit A/D Converter," *IEEE Trans. Instrum. Meas.*, vol. 63, no. 1, pp. 56-62, Jan. 2014.
[21] P. Sovilj *et al.*, "Stochastic Measurement of Reactive Power Using a Two-bit A/D Converter", *Proc. IMEKO TC-4 Int. Symp. on Understanding the World through Electrical and Electronic Measurement*, pp. 176-179, Sept. 2016.
[22] M. Urekar *et al.*, "Accuracy Improvement of the Stochastic Digital Electrical Energy Meter," *Measurement*, vol. 98, pp. 139-150, Feb. 2017.
[23] V. Vujicic, I. Zupunski and S. Milovancev, "Predetermination of the Quantization Error in Digital Measurement Systems," *IEEE Trans. Instrum. Meas.*, vol. 46, no. 2, pp. 439-441, Apr. 1997.
[24] R. B. Staszewski and P. T. Balsara, "All-Digital PLL with Ultra Fast Settling," *IEEE Trans. Circuits Syst. II*, vol. 54, no. 2, pp. 181-185, Feb. 2007.
[25] C. Lu 1, L. Huang and W. Li, "A 2-Bit 4GS/s Flash A/D Converter in 0.18 μm CMOS for an IR-UWB Communication System," *9th Int, Conference on Solid-State and Integrated-Circuit Technology*, pp. 1965-1968, Oct. 2008.
[26] R. Li *et al.* "A 14-Bit 2-GS/s DAC with SFDR > 70dB up to 1-GHz in 65-nm CMOS," *9th IEEE 9th Int. Conference on ASIC*, pp. 500-503, Oct. 2011.
[27] Z. Mitrovic, "A Phase Angle Standard," *Meas. Sci. Technol.*, vol. 15, no. 3, pp. 559-564, Mar. 2004.
[28] H. Lev-Ari and A. Stankovic, "A Decomposition of Apparent Power in Polyphase Unbalanced Networks in Nonsinusoidal Operation," *IEEE Trans. Power Systems*, vol. 21, no. 1, pp. 438-440, Feb. 2006.
[29] S. Pajic and A. Emanuel, "Modern Apparent Power Definitions: Theoretical Versus Practical Approach - The General Case," *IEEE Trans. Power Delivery*, vol. 21, no. 4, pp. 1787-1792, Oct. 2006.
[30] H. Lev-Ari and A. Stankovic (2015, Sept.). Electric Power Quality. [Online] Available: http://web.eecs.utk.edu/~dcostine/ECE620/Fall2015/lectures/CURENT_talk_combined.pdf
[31] L. Czarnecki and P. Haley, "Power Properties of Four-Wire Systems at Nonsinusoidal Supply Voltage," IEEE Trans. Power Delivery, vol. 31, no. 2, pp. 513-521, Apr. 2016.
[32] H. Lev-Ari and A. Stankovic "Electric Power Quality," CURENT & NUCEER Centers, Northeastern University, Sept. 2017.
[33] S. C. Ferreira *et al.*, "Adaptive Real-time Power Measurement Based on IEEE Standard 1459-2010," *Electr. Pow. Compo. Systems*, vol. 43 no. 11, pp. 1307-1317, Jun 2015.
[34] *IEEE Standard Definitions for the Measurement of Electric Power Quantities Under Sinusoidal, Nonsinusoidal, Balanced, or Unbalanced Conditions,* IEEE Std 1459™-2010.

# APPENDIX A

*- The Calculation of Reactive Power over Fourier Coefficients -*

Let $u(t)$ and $i(t)$ be continuous periodic functions over the time interval $T$. Based on the Weierstrass approximation theorem, these functions can be approximated with polynomials

$$u(t) \approx u(t,M) = \sum_{j=1}^{M} \left[ a_j \cdot cos(j\omega t) + b_j \cdot sin(j\omega t) \right] \tag{A.1}$$

$$i(t) \approx i(t,M) = \sum_{j=1}^{M} \left[ c_j \cdot cos(j\omega t) + d_j \cdot sin(j\omega t) \right] \tag{A.2}$$

where $\omega = \frac{2\pi}{T}$.

The functions $u(t)$ and $i(t)$ can be also expressed in the form:

$$u(t, M) = \sum_{j=1}^{M} \sqrt{2} \cdot U_j \cdot sin\left[ (j\omega t) + \varphi_{j(u)} \right] \tag{A.3}$$

$$i(t, M) = \sum_{j=1}^{M} \sqrt{2} \cdot I_j \cdot sin\left[ (j\omega t) + \varphi_{j(i)} \right] \tag{A.4}$$

where $U_j^{\,2} = \frac{a_j^{\,2} + b_j^{\,2}}{2}$, $I_j^{\,2} = \frac{c_j^{\,2} + d_j^{\,2}}{2}$, $\varphi_{j(u)} = arctg(\frac{b_j}{a_j})$, $\varphi_{j(i)} = arctg(\frac{d_j}{c_j})$ and $1 \le j \le M$.

Now we can state the next theorem.

**Theorem 1**. *For any $M \ge 1$ it holds that*

$$Q_{(B)} = \sum_{j=1}^{M} Q_{j\,(B)} = \sum_{j=1}^{M} U_j \cdot I_j \cdot sin\,\varphi_j = \sum_{j=1}^{M} \frac{a_j \cdot d_j - b_j \cdot c_j}{2}$$

**Proof.** We adopt mathematical induction to prove Theorem 1.

**Step 1**. For $M = k = 1$, we have

$$u(t,1) = \sqrt{2} \cdot U_1 \cdot sin\left[ (\omega t) + \varphi_{1(u)} \right]$$

$$i(t,1) = \sqrt{2} \cdot I_1 \cdot sin\left[ (\omega t) + \varphi_{1(i)} \right]$$

where $\varphi_1 = \varphi_{1(u)} - \varphi_{1(i)}$.

Without loss of generality, suppose that $\varphi_{1(u)} = 0$. In that case, we can write

$$u(t,1) = \sqrt{2} \cdot U_1 \cdot sin(\omega t)$$

$$i(t,1) = \sqrt{2} \cdot I_1 \cdot sin\,(\omega t - \varphi_1)$$

Now, by using the identity principle for polynomials, we get

$$a_1 = 0$$

$$b_1 = \sqrt{2} \cdot U_1$$

$$c_1 = -\sqrt{2}\cdot I_1\cdot \sin\varphi_1$$

$$d_1 = \sqrt{2}\cdot I_1\cdot \cos\varphi_1$$

Hence, it follows that

$$\frac{a_1\cdot d_1 - b_1\cdot c_1}{2} = \frac{0\cdot\sqrt{2}\cdot I_1\cdot\cos\varphi_1 - \sqrt{2}\cdot U_1\cdot(-\sqrt{2}\cdot I_1\cdot \sin\varphi_1)}{2} = U_1\cdot I_1\cdot \sin\varphi_1 = Q_{1(\mathrm{B})}$$

**Step 2**. Assume that Theorem 1 holds for $M = k \geq 2$. Then for $M = k + 1$, we have

$$u(t,k+1) = \sum_{j=1}^{k+1}\left[a_j\cdot\cos(j\omega t) + b_j\cdot\sin(j\omega t)\right]$$

$$i(t,k+1) = \sum_{j=1}^{k+1}\left[c_j\cdot\cos(j\omega t) + d_j\cdot\sin(j\omega t)\right].$$

Hence, we can write

$$u(t,k+1) = u(t,k) + a_{k+1}\cdot\cos(k+1)\omega t + b_{k+1}\cdot\sin(k+1)\omega t$$

$$i(t,k+1) = i(t,k) + c_{k+1}\cdot\cos(k+1)\omega t + d_{k+1}\cdot\sin(k+1)\omega t$$

i.e.,

$$u(t,k+1) = u(t,k) + \sqrt{2}\cdot U_{k+1}\cdot\sin\left[(k+1)\omega t + \varphi_{k+1(u)}\right]$$

$$i(t,k+1) = i(t,k) + \sqrt{2}\cdot I_{k+1}\cdot\sin\left[(k+1)\omega t + \varphi_{k+1(i)}\right].$$

According to the inductive assumption, the expression

$$Q_{(\mathrm{B})} = \sum_{j=1}^{k+1}\frac{a_j\cdot d_j - b_j\cdot c_j}{2}$$

is valid. So, for $M = k + 1$ is

$$Q_{(\mathrm{B})} = \sum_{j=1}^{k} U_j\cdot I_j\cdot\sin\varphi_j + \frac{a_{k+1}\cdot d_{k+1} - b_{k+1}\cdot c_{k+1}}{2}.$$

With this in mind, suppose that $\varphi_{k+1(u)} = 0$, where $\varphi_{k+1} = \varphi_{k+1(u)} - \varphi_{k+1(i)}$. In that case, it holds that

$$u(t,k+1) = u(t,k) + \sqrt{2}\cdot U_{k+1}\cdot\sin(k+1)\omega t$$

$$i(t,k+1) = i(t,k) + \sqrt{2}\cdot I_{k+1}\cdot\sin\left[(k+1)\omega t - \varphi_{k+1}\right].$$

Now, by using the identity principle for polynomials, we get

$$a_{k+1} = 0$$

$$b_{k+1} = \sqrt{2}\cdot U_{k+1}$$

$$c_{k+1} = -\sqrt{2}\cdot I_{k+1}\cdot\sin\varphi_{k+1}$$

$$d_{k+1} = \sqrt{2}\cdot I_{k+1}\cdot\cos\varphi_{k+1}$$

Hence, it follows that

$$Q_{(\mathrm{B})}=\sum_{j=1}^{k}U_j\cdot I_j\cdot \sin\varphi_j+\frac{a_{k+1}\cdot d_{k+1}-b_{k+1}\cdot c_{k+1}}{2}=\sum_{j=1}^{k}U_j\cdot I_j\cdot \sin\varphi_j+U_{k+1}\cdot I_{k+1}\cdot \sin\varphi_{k+1}=\sum_{j=1}^{k+1}U_j\cdot I_j\cdot \sin\varphi_j\,.\,\square$$

**Theorem 2**. *For any M ≥ 1 it holds that*

$$Q_{(-\pi/2)}=\sum_{j=1}^{M}Q_{j\,(-\pi/2)}=Q_{(\mathrm{B})}=\sum_{j=1}^{M}Q_{j\,(\mathrm{B})}$$

**Proof.** In non-sinusoidal regime, the active power is calculated as

$$P=\frac{1}{T}\cdot\int_0^T u(t)\cdot i(t)\,dt=\sum_{j=1}^{M}P_j=\sum_{j=1}^{M}U_j\cdot I_j\cdot\cos\varphi_j$$

If the voltage lags the current by $\pi/2$ (at each harmonic frequency), then, by the definition [10], $Q_{(-\pi/2)}$ is calculated as

$$Q_{(-\pi/2)}=\frac{1}{T}\cdot\int_0^T u(t)_{(-\pi/2)}\cdot i(t)\,dt=P_{(-\pi/2)}=\sum_{j=1}^{M}U_j\cdot I_j\cdot\cos(\varphi_j-\pi/2)$$

However, since $\cos(\varphi_j-\pi/2)=\sin\varphi_j$, it follows that

$$P_{(-\pi/2)}=\sum_{j=1}^{M}U_j\cdot I_j\cdot\sin\varphi_j=\sum_{j=1}^{M}Q_{j\,(\mathrm{B})}=Q_{(\mathrm{B})}\,.\,\square$$

We remark, without detailed proof, that in the special case (when the phase angle between the first harmonic of the voltage and current is positive) Budeanu's definions of RP at the fundamental frequency ($M$ = 1) is equivalent to that of Fryze. Namely, from the expression

$$Q_{(\mathrm{F})}=\sqrt{U^2I^2-P^2}=\sqrt{\left(\sum_{j=1}^{M}U_j^{\,2}\right)\cdot\left(\sum_{j=1}^{M}I_j^{\,2}\right)-\left(\sum_{j=1}^{M}U_jI_j\cos\varphi_j\right)^2}$$

it is clear that

$$Q_{(\mathrm{F})}=\sqrt{\left(\sum_{j=1}^{M}\frac{a_j^{\,2}+b_j^{\,2}}{2}\right)\cdot\left(\sum_{j=1}^{M}\frac{c_j^{\,2}+d_j^{\,2}}{2}\right)-\left(\sum_{j=1}^{M}\frac{a_jc_j+b_jd_j}{2}\right)^2}$$

Thus, it is easy to show that

$$Q_{1\,(\mathrm{B})}=U_1\cdot I_1\cdot\sin\varphi_1\le Q_{1\,(\mathrm{F})}=U_1\cdot I_1\cdot\left|\sin\varphi_1\right|.$$

# APPENDIX B

*- Uncertainty of the Measurement of Reactive Energy -*

The total reactive energy $E_R$ is calculated as

$$E_R = \bar{Q} \cdot T \tag{B.1}$$

where $\bar{Q}$ represents the mean reactive power over the time interval $T$. Now, let $dE_R$ be the uncertainty of the measurement of total reactive energy. In that case it follows that

$$dE_R = d\bar{Q} \cdot T + \bar{Q} \cdot dT \tag{B.2}$$

Based on this, it is easy to see that the relative uncertainty of the measurement of total reactive energy can be expressed as

$$\frac{dE_R}{E_R} = \frac{d\bar{Q} \cdot T + \bar{Q} \cdot dT}{\bar{Q} \cdot T} = \frac{d\bar{Q}}{\bar{Q}} + \frac{dT}{T} \tag{B.3}$$

However, as the relative uncertainty of the time measurement is very small ($dT/T < 10^{-6}$ when $T \geq 1$s), it is clear that

$$\frac{dE_R}{E_R} = \frac{d\bar{Q}}{\bar{Q}} \tag{B.4}$$

Highlights

The proposed hardware is extremely simple, reliable and accurate.

The proposed measurements are completely parallel.

The proposed signal processing is completely parallel too.

The described idea provides accurate measurements over a very wide frequency range.

All above mentioned is practically applied and presented in the paper.